Journal of Power Sources 195 (2010) 4375–4379

Contents lists available at ScienceDirect

Journal of Power Sources

journal homepage: www.elsevier.com/locate/jpowsour

Short Communication

Nitrogen-doped mesoporous carbon for energy storage in vanadium redox flow batteries

Yuyan Shao[a,*], Xiqing Wang[b], Mark Engelhard[a], Chongmin Wang[a], Sheng Dai[b], Jun Liu[a], Zhenguo Yang[a], Yuehe Lin[a,*]

[a] Pacific Northwest National Laboratory, Richland, WA 99352, USA
[b] Oak Ridge National Laboratory, Oak Ridge, TN 37831, USA

ARTICLE INFO

Article history:
Received 3 November 2009
Received in revised form 5 January 2010
Accepted 6 January 2010
Available online 14 January 2010

Keywords:
Vanadium redox flow battery
Renewable energy storage
Nitrogen-doped mesoporous carbon
Electron transfer
Reversibility
Energy efficiency

ABSTRACT

We demonstrate an excellent performance of nitrogen-doped mesoporous carbon (N-MPC) for energy storage in vanadium redox flow batteries. Mesoporous carbon (MPC) is prepared using a soft-template method and doped with nitrogen by heat-treating MPC in NH_3. N-MPC is characterized with X-ray photoelectron spectroscopy and transmission electron microscopy. The redox reaction of $[VO]^{2+}/[VO_2]^+$ is characterized with cyclic voltammetry and electrochemical impedance spectroscopy. The electrocatalytic kinetics of the redox couple $[VO]^{2+}/[VO_2]^+$ is significantly enhanced on N-MPC electrode compared with MPC and graphite electrodes. The reversibility of the redox couple $[VO]^{2+}/[VO_2]^+$ is greatly improved on N-MPC (0.61 for N-MPC vs. 0.34 for graphite), which is expected to increase the energy storage efficiency of redox flow batteries. Nitrogen doping facilitates the electron transfer on electrode/electrolyte interface for both oxidation and reduction processes. N-MPC is a promising material for redox flow batteries. This also opens up new and wider applications of nitrogen-doped carbon.

1. Introduction

The fast development of renewable energy (wind energy, solar energy, etc.) has made the scientific research on electrochemical energy storage more important and more urgent than ever [1]. Energy storage has been the Achilles' Heel of renewable energy [2]. Due to the intermittence of wind and solar energy, energy storage is necessary to level the fluctuation of power generation and makes it match power demand [3,4]. Redox flow batteries [4–7] have been proposed as a promising grid energy storage system for renewable energy due to its low cost, modularity configuration, flexible operation, and fast power response [8].

A redox flow battery is an electrochemical energy system that, rather than storing energy at the electrodes like lithium batteries, stores electric energy in two separated solutions containing different redox couples with different electrochemical potentials [8]. Several redox couple-based flow battery systems have been proposed and developed (e.g., bromide/polysulphide [5,9,10], Mn(II)/Mn(III) [11], Ce(III)/Ce(IV) [12,13], soluble Pb battery [14]), among which the all-vanadium redox flow battery ($[VO]^{2+}/[VO_2]^+$ [positive] –V^{3+}/V^{2+} [negative] redox couples) [15] is the most developed one [7,16,17] due to its low cost, high energy efficiency and long service lifetime. The most important advantage of all-vanadium redox flow battery is the use of the same element (vanadium) in both half-cells that greatly alleviates the problem with cross-contamination of the two half-cell electrolytes [8,18]. The cross-contamination of electrolytes is the main degradation model of redox flow batteries. It has been shown that the redox reaction of V(II)/V(III) couple (negative side) is more reversible and the reaction kinetics is much faster [19–21]. However, the kinetics of the $[VO]^{2+}/[VO_2]^+$ reaction is much slower and more complex which involves at least three elementary steps (i.e. one electron transfer and two proton exchanges) and several complex intermediates depending on the electrolyte pH and potentials [20,22]. Therefore, the electrochemical kinetics limitation of vanadium redox flow batteries is in the positive side ($[VO]^{2+}/[VO_2]^+$ redox couple). It is important to develop novel electrodes with high catalytic activity toward $[VO]^{2+}/[VO_2]^+$ redox reaction. Currently, the most widely used electrodes for redox flow batteries are graphite-based materials [23] such as graphite felt [17,18], graphite powder [16], and carbon black [24,25].

Nitrogen-doped carbon nanostructured materials have been shown to exhibit higher electrocatalytic activity in many electrochemical devices such as fuel cells [26–31] and biosensors [32]. Here we study the electrochemical redox behavior of $[VO]^{2+}/[VO_2]^+$ couple on nitrogen-doped mesoporous carbon (N-MPC) electrode, which shows much higher performance than the widely used graphite.

* Corresponding authors. Tel.: +1 509 371 6228.
E-mail addresses: yuyan.shao@gmail.com (Y. Shao), yuehe.lin@pnl.gov (Y. Lin).

0378-7753/$ – see front matter © 2010 Elsevier B.V. All rights reserved.
doi:10.1016/j.jpowsour.2010.01.015

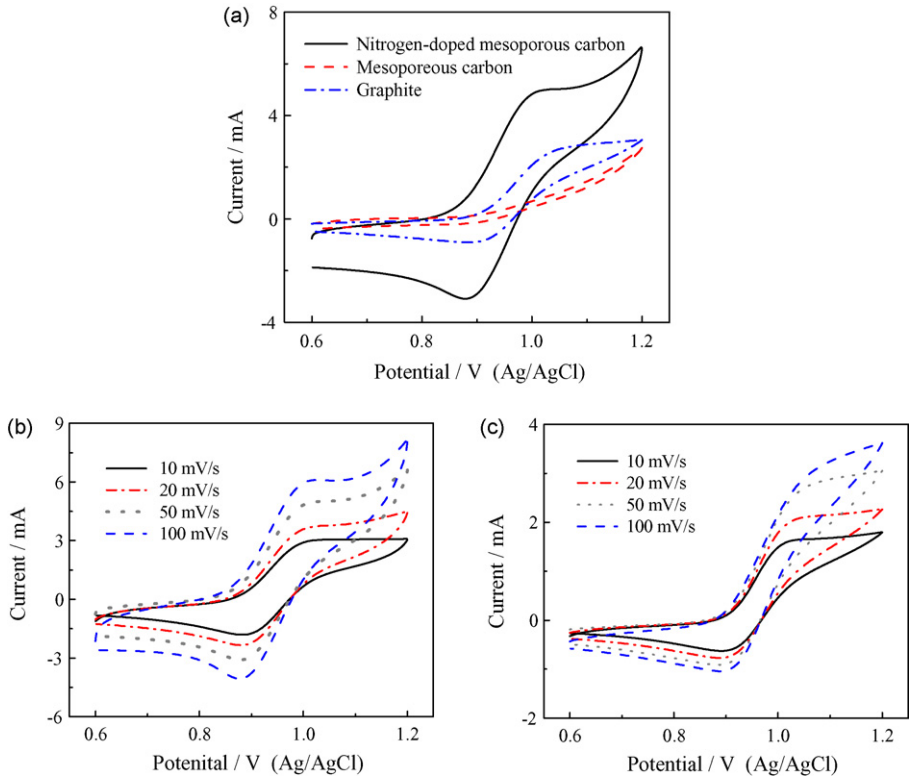

Fig. 1. (a) Cyclic voltammograms (CV) on different electrodes in 3.0 M H_2SO_4 + 1.0 M $VOSO_4$ (50 mV/s); CVs on nitrogen-doped mesoporous carbon (b) and graphite (c) electrodes at various scanning rates in 3.0 M H_2SO_4 + 1.0 M $VOSO_4$.

2. Experimental

2.1. Chemicals and materials

$VOSO_4$, 5 wt% Nafion solution, and sulphuric acid were obtained from Sigma–Aldrich and used as received without further purification. Graphite powder (~40 μm, Sigma–Aldrich) was attrition-milled in 2-propanol for 2 h to further decrease the particle size (200–300 nm) and increase the active surface area.

Nitrogen-doped mesoporous carbon (N-MPC) was prepared by heat-treating the mesoporous carbon (MPC) in NH_3 atmosphere, and the MPC was prepared using a soft-template method [33]. In brief, 1.25 g phloroglucinol and 1.25 g polyethyleneoxide-b-polypropyleneoxide-b-polyethyleneoxide (Pluronic F127 $EO_{106}PO_{70}EO_{106}$) were dissolved in 9.0 g of a mixture of ethanol and water (10:9 in weight), then 0.1 g 37% HCl was added and the solution was stirred for half an hour. 1.3 g of 37% formaldehyde solution was then added to the mixture in one batch and stirred for 1 h. A polymer layer was separated from the reactants by centrifugation and cast into a thin film on a Petri dish. The film was first cured overnight at room temperature and then further cured overnight at 100 °C. The cured film was scratched off the Petri dish and carbonized under nitrogen in a tubular furnace via heating ramps of 1 °C min^{-1} from 100 to 400 °C and 5 °C min^{-1} from 400 to 850 °C and kept at 850 °C for 2 h. The obtained MPC was then heat-treated in NH_3 atmosphere at 850 °C for 2 h to produce N-MPC. The specific surface area of N-MPC and MPC are about 1100 m^2 g^{-1} and 500 m^2 g^{-1}, respectively.

2.2. Materials characterization

The TEM images of N-MPC were taken on a JEOL TEM 2010 microscope equipped with an Oxford ISIS system. The operating voltage on the microscope was 200 keV. All images were digitally recorded with a slow-scan CCD camera. The XPS measurements were carried out on the Physical Electronics Quantum 2000 Scanning ESCA Microprobe. This system used a focused monochromatic aluminum Kα X-ray (1486.6 eV) source and a spherical section analyzer. The X-ray beam used was a 100 W, 100-mm diameter beam rastered over a 1.3-mm by 0.2-mm area on the sample. Wide-scan data were collected using pass energy of 117.4 eV. The samples were dried in vacuum before XPS test.

2.3. Electrochemical tests

The cyclic voltammetry (CV) and the electrochemical impedance spectroscopy (EIS, 1–10^5 Hz, amplitude = 5 mV) tests were carried out in 3.0 M H_2SO_4 + 1.0 M $VOSO_4$ solution using a three-electrode cell which was controlled with a CHI660C workstation (CH Instruments, USA). In order to study the reduction process of the $[VO]^{2+}/[VO_2]^{+}$ redox couple, 3.0 M H_2SO_4 + 1.0 M $VOSO_4$ solution was first oxidized at 1.0 V [34] and then the EIS was carried out. A Pt wire and Ag/AgCl electrode were used as the counter and reference electrodes, respectively. The working electrode was prepared by applying highly dispersed carbon ink onto the pre-polished glass carbon disk electrode. A Nafion thin film was formed on the surface by dropping 10 μL 0.05 wt% Nafion on it after the ink was dried. The carbon ink was prepared by dispersing carbon powder (graphite, MPC, N-MPC powder) in ethanol under strong ultrasonication. Carbon loading on the disk electrode is 20 μg.

3. Results and discussion

Fig. 1a shows the cyclic voltammograms (CV) on nitrogen-doped mesoporous carbon (N-MPC), mesoporous carbon (MPC) and

graphite electrodes. The redox peaks (0.85–1.05 V) are attributed to the following reversible reaction [8].

$$[VO]^{2+} + H_2O \leftrightarrow [VO_2]^{+} + 2H^{+} + e^{-} \quad (1)$$

The electrocatalytic activity (peak currents/peak potentials and onset potentials of redox reactions) and the reversibility of reaction (I) are the key criteria in evaluating the performance of an electrode for a redox flow battery. It can be seen from CVs in Fig. 1a that the onset potentials of the oxidation process are 0.82, 0.89 and 0.91 V on N-MPC, graphite and MPC electrodes, respectively, which means that the electrocatalytic kinetics of the oxidation process in reaction (I) on the electrodes are in the order of N-MPC > graphite > MPC. The lower oxidation potential is beneficial for improving the energy storage efficiency because it implies a lower charge voltage for the redox flow battery (the energy storage efficiency of a battery is in direct proportion to the ratio of discharge/charge voltages) [8]. The redox peak current (Fig. 1a) is much higher on N-MPC than that on graphite electrode, and no obvious redox peak on MPC electrode. Therefore, N-MPC exhibits the highest electrocatalytic activity toward reaction (I). The reversibility of reaction (I) can be estimated from the ratio of the reduction peak current and the oxidation peak current, which is 0.61 and 0.34 for N-MPC and graphite respectively (calculated from Fig. 1a with background subtraction, no data available for MPC electrode because of no obvious peak currents).

The reversibility of reaction (I) can also be characterized with the peak potenitals. Fig. 1b and c shows the CVs at various scanning rates on N-MPC and graphite electrodes respectively. The peak potentials for the redox reactions of $[VO]^{2+}/[VO_2]^{+}$ on N-MPC keep almost unchanged with increasing potential scanning rates, indicating that the redox reactions of $[VO]^{2+}/[VO_2]^{+}$ is quite reversible on N-MPC electrode. However, the anodic (cathodic) peak potentials shift positively (negatively) on graphite electrode with increasing potential scanning rates, which implies that the reversibility of reaction (I) on graphite electrode is poorer than that on N-MPC.

Fig. 2 shows the electrochemical impedance spectroscopy (EIS) (Nyquist plots) of different electrodes in 3.0 M H_2SO_4 + 1.0 M $VOSO_4$ solution at 1.0 V (a) and in anodically oxidized 3.0 M H_2SO_4 + 1.0 M $VOSO_4$ solution at 0.9 V (b). Based on the CV (Fig. 1a), the reaction at 1.0 V corresponds to the oxidation process of $[VO]^{2+}/[VO_2]^{+}$ and the reaction at 0.9 V corresponds to the reduction process of $[VO]^{2+}/[VO_2]^{+}$. Z' (~3.5 Ω) at $Z''=0$ is the ohmic resistance that combines the solution, electrode and the contact resistance. It keeps almost constant for N-MPC and MPC, but slightly smaller for graphite electrode which might be due to the high conductivity of graphite. The first arc (high frequency range) in the Nyquist plots is due to the charge transfer reaction at the electrolyte/electrode interface, the radius of which reflects the charge transfer (reaction) resistance [17]: the smaller arc radius implying the faster reaction (the lower reaction resistance). It can be seen that the reaction resistance is always in the order of N-MPC ≪ graphite ≪ MPC. This is consistent with the CV results. Therefore both EIS and CV results show that both the reduction and oxidation processes of $[VO]^{2+}/[VO_2]^{+}$ redox couple are enhanced on N-MPC electrode.

Fig. 3a shows the survey XPS spectra of N-MPC, MPC and graphite. The XPS spectra are very clean for all the three carbon samples (without any metal impurities such as Fe, Co, Ni which might affect the catalytic activity of carbon electrodes [35]). Nitrogen was observed only on N-MPC (nitrogen content of 3.3% calculated from the XPS data). The oxygen signal in the spectrum of graphite is due to the oxidation of graphite during the strong milling process and the adsorption of oxygen on the defects of milled graphite. Based on the signal intensity of oxygen and carbon in the XPS spectra, the oxygen content is in the order of MPC > graphite > N-MPC. The oxygen content in mesoporous carbon significantly decreases after

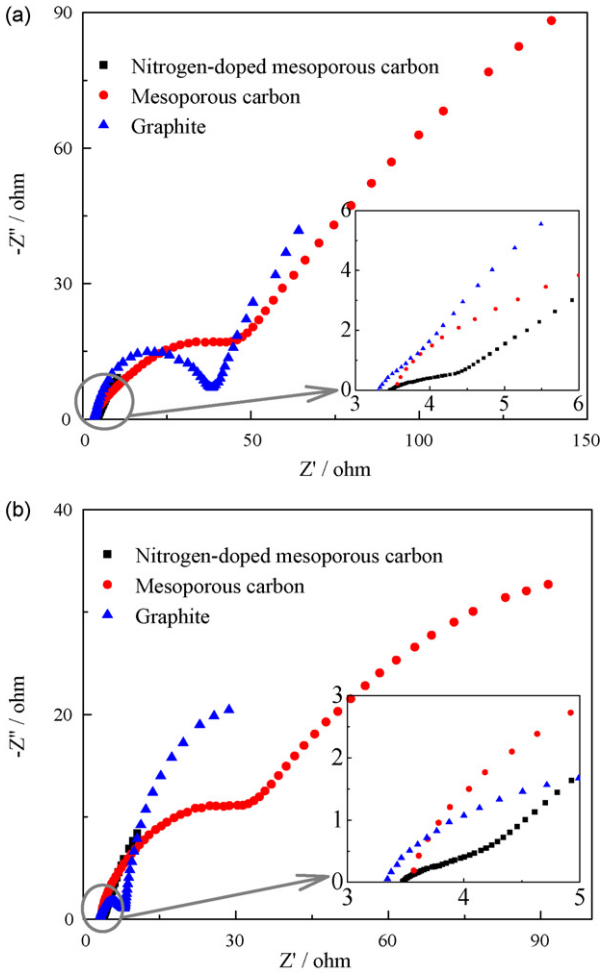

Fig. 2. Electrochemical impedance spectroscopy (EIS) of different electrodes in 3.0 M H_2SO_4 + 1.0 M $VOSO_4$ solution at 1.0 V (a) and in anodically oxidized 3.0 M H_2SO_4 + 1.0 M $VOSO_4$ solution at 0.9 V (b).

NH_3 treatment. This might be due to the decomposition of oxygen-containing groups at high temperature (850 °C) [36,37] and the reaction between NH_3 and oxygen-containing groups [38]. Fig. 3b shows the N1s high-resolution XPS of N-MPC which reveals several nitrogen functional groups [39,40]: pyridinic-N (N1, BE (binding energy) = 398.7 ± 0.2 eV), pyrrolic-N (N2, BE = 400.3 ± 0.2 eV), quaternary nitrogen (N3, BE = 401.2 ± 0.2 eV), N-oxides of pyridinic-N (N4, BE = 402.8 ± 0.4 eV). The molecular structures (chemical states) of these nitrogen functional groups can be described as the following [40,41]: pyridinic-N (N1) refers to the nitrogen atom on the edge of graphene planes, which is bonded to two carbon atoms and donates one p electron to the aromatic π system; Pyrrolic-N (N2) refers to the nitrogen atom that is bonded to two carbon atoms and contributes to the π system with two p-electrons; quaternary nitrogen (N3) can be described as "graphitic nitrogen" or "substituted nitrogen", in which nitrogen is incorporated into the graphene layer and replaces a carbon atom within a graphene plane; N-oxides of pyridinic-N (N4) are bonded to two carbon atoms and one oxygen atom, and can be termed as pyridinic $-(N^{+}-O^{-})$.

If we compare the properties of N-MPC and graphite, in addition to nitrogen doping, they are different in several aspects (for example, the specific surface area, the pore sizes and distribution, the graphitic structures). Each of these factors might contribute to their difference in the electrochemical performance. However, if we compare MPC and N-MPC, the main difference is in the nitrogen doping and the oxygen content. It is known [42–45] that

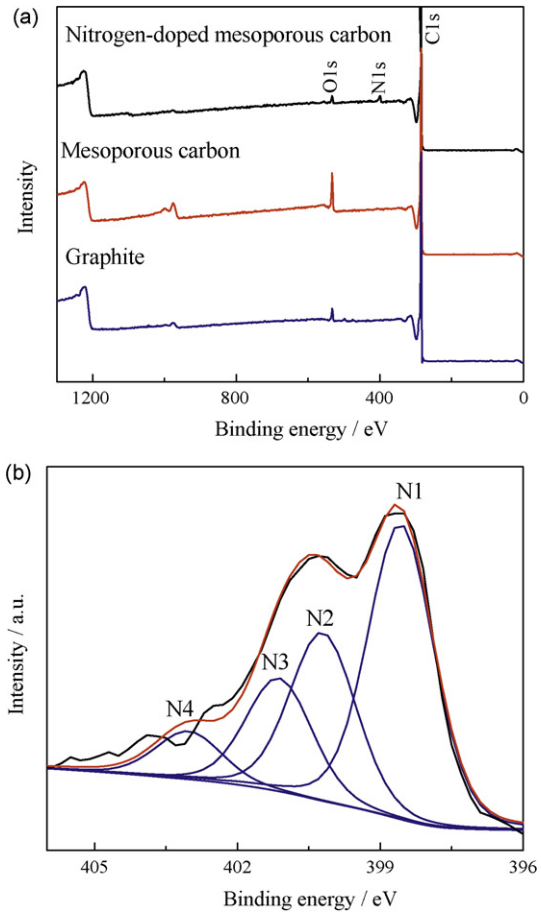

Fig. 3. (a) Survey XPS spectra of graphite, mesoporous carbon, and nitrogen-doped mesoporous carbon; (b) N1s XPS spectra of nitrogen-doped mesoporous carbon.

oxygen-containing groups accelerate the electron transfer and the electrocatalytic activity of carbon electrodes (N-MPC is the lowest in oxygen content). Therefore, the higher electrocatalytic activity and the more reversibility of reaction (I) on N-MPC are only attributable to the nitrogen doping. Nitrogen doping [27] has been shown to improve the electrocatalytic activity of carbon nanostructures toward, for example, oxygen reduction [26,28,29,31], methanol oxidation [46,47], and H_2O_2 reduction [32]. It has been shown through density functional theory (DFT) calculations that carbon atoms adjacent to nitrogen dopants possess a substantially high positive charge density to counterbalance the strong electronic affinity of the nitrogen atom [28]. The "positively charged" carbon atoms work as the active sites for the oxidation reaction (electrons are transferred from the reactants to the electrode). The five valence electrons of nitrogen atoms contribute the extra charge to the π bond in graphene layers (e.g., pyridinic-N possesses one lone pair of electrons in addition to the one electron donated to the conjugated π bond system), which enhances the basicity of carbon [48,49] and the electrical conductivity of nitrogen-doped carbon [50]. This is beneficial for the reduction process (electrons are transferred from the electrode to the reactant). The redox process of $[VO]^{2+} \leftrightarrow [VO_2]^{+}$ involves the breaking and formation of V–O bonds [20,51]. The nitrogen-induced charge delocalization might also change the chemisorption mode of V/O atoms on carbon, like in the case of oxygen reduction [28] and decrease the activation energy for vanadium–oxygen bond formation and breaking, which facilitates the redox process.

In addition, nitrogen doping also changes the wetting property of mesoporous carbon and makes N-MPC more hydrophilic

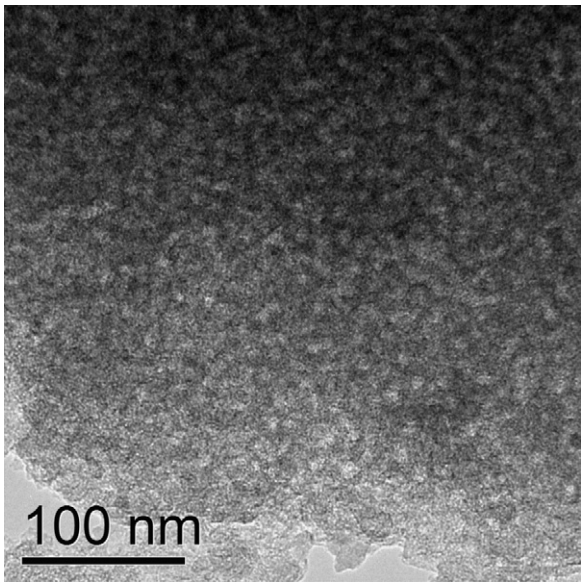

Fig. 4. TEM image of nitrogen-doped mesoporous carbon.

[52] which increases the electrochemically active sites. TEM image (Fig. 4) shows that the pore sizes of N-MPC are 6–10 nm. This is beneficial for mass transfer.

4. Conclusions

In summary, we have demonstrated a novel electrode material with significantly enhanced performance for energy storage application in vanadium redox flow batteries: nitrogen-doped mesoporous carbon (N-MPC). The reaction kinetics and reversibility of $[VO]^{2+}/[VO_2]^{+}$ redox couple, which is considered to be the controlling reaction in vanadium redox flow batteries, are greatly improved on N-MPC electrode compared with undoped mesoporous carbon and graphite electrodes, which is expected to increase the energy storage efficiency. The enhanced catalytic activity is attributable to nitrogen doping which makes both the electrochemical oxidation and reduction reactions facile on carbon electrodes. N-MPC is a promising electrode material for vanadium redox flow batteries. This work presents new chemistry on and opens up wider applications of nitrogen-doped carbon materials, in addition to the traditional applications for oxygen reduction [27,28] and the oxidation/reduction of small molecules (methanol [30,47], H_2O_2 [32]).

Acknowledgements

This work is partially supported by a Laboratory Directed Research and Development program at Pacific Northwest National Laboratory (PNNL). Part of the research described in this paper was performed at the Environmental Molecular Sciences Laboratory, a national scientific-user facility sponsored by the U.S. Department of Energy's (DOE's) Office of Biological and Environmental Research and located at PNNL. PNNL is operated for U.S. DOE by Battelle under Contract DE-AC05-76RL01830. J. Liu and Z. G. Yang acknowledge the support from Office of Electricity Delivery&Energy Reliability's Storage Program.

References

[1] J.B. Goodenough, H.D. Abruña, M.V. Buchanan, Steven Visco, M. Stanley Whittingham, B. Dunn, Y. Gogotsi, A. Gewirth, D. Nocera, R.D. Kelley, J.S. Vetrano, Report of the Basic Energy Sciences Workshop for Electrical Energy Storage, April 2–4, 2007. http://www.sc.doe.gov/bes/reports/files/EES_rpt.pdf.

[2] B.S. Lee, D.E. Gushee, Chem. Eng. Prog. 104 (2008) S29–S32.
[3] M.S. Whittingham, MRS Bull. 33 (2008) 411–419.
[4] L. Joerissen, J. Garche, C. Fabjan, G. Tomazic, J. Power Sources 127 (2004) 98–104.
[5] P. Zhao, H.M. Zhang, H.T. Zhou, B.L. Yi, Electrochim. Acta 51 (2005) 1091–1098.
[6] C. Fabjan, J. Garche, B. Harrer, L. Jorissen, C. Kolbeck, F. Philippi, G. Tomazic, F. Wagner, Electrochim. Acta 47 (2001) 825–831.
[7] K.L. Huang, X.G. Li, S.Q. Liu, N. Tan, L.Q. Chen, Renewable Energy 33 (2008) 186–192.
[8] C. Ponce de Leon, A. Frias-Ferrer, J. Gonzalez-Garcia, D.A. Szanto, F.C. Walsh, J. Power Sources 160 (2006) 716–732.
[9] D.P. Scamman, G.W. Reade, E.P.L. Roberts, J. Power Sources 189 (2009) 1231–1239.
[10] Y.Y. Shao, M. Engelhard, Y.H. Lin, Electrochem. Commun. 11 (2009) 2064–2067.
[11] F.Q. Xue, Y.L. Wang, W.H. Wang, X.D. Wang, Electrochim. Acta 53 (2008) 6636–6642.
[12] B. Fang, S. Iwasa, Y. Wei, T. Arai, M. Kumagai, Electrochim. Acta 47 (2002) 3971–3976.
[13] Y. Liu, X. Xia, H. Liu, J. Power Sources 130 (2004) 299–305.
[14] D. Pletcher, R. Wills, Phys. Chem. Chem. Phys. 6 (2004) 1779–1785.
[15] M. Skyllaskazacos, M. Rychcik, R.G. Robins, A.G. Fane, M.A. Green, J. Electrochem. Soc. 133 (1986) 1057–1058.
[16] H.Q. Zhu, Y.M. Zhang, L. Yue, W.S. Li, G.L. Li, D. Shu, H.Y. Chen, J. Power Sources 184 (2008) 637–640.
[17] W.H. Wang, X.D. Wang, Electrochim. Acta 52 (2007) 6755–6762.
[18] M. Skyllas-Kazacos, J. Power Sources 124 (2003) 299–302.
[19] M.H. Chakrabarti, R.A.W. Dryfe, E.P.L. Roberts, Electrochim. Acta 52 (2007) 2189–2195.
[20] M. Gattrell, J. Park, B. MacDougall, J. Apte, S. McCarthy, C.W. Wu, J. Electrochem. Soc. 151 (2004) A123–A130.
[21] S. Zhong, M. Skyllaskazacos, J. Power Sources 39 (1992) 1–9.
[22] N. Kausar, R. Howe, M. Skyllas-Kazacos, J. Appl. Electrochem. 31 (2001) 1327–1332.
[23] H.T. Zhou, H.M. Zhang, P. Zhao, B.L. Yi, Electrochim. Acta 51 (2006) 6304–6312.
[24] Y.M. Zhang, Q.M. Huang, W.S. Li, H.Y. Peng, S.J. Hu, J. Inorg. Mater. 22 (2007) 1051–1055.
[25] G.J.W. Radford, J. Cox, R.G.A. Wills, F.C. Walsh, J. Power Sources 185 (2008) 1499–1504.
[26] S. Maldonado, K.J. Stevenson, J. Phys. Chem. B 109 (2005) 4707–4716.
[27] Y.Y. Shao, J.H. Sui, G.P. Yin, Y.Z. Gao, Appl. Catal. B: Environ. 79 (2008) 89–99.
[28] K.P. Gong, F. Du, Z.H. Xia, M. Durstock, L.M. Dai, Science 323 (2009) 760–764.
[29] R.A. Sidik, A.B. Anderson, N.P. Subramanian, S.P. Kumaraguru, B.N. Popov, J. Phys. Chem. B 110 (2006) 1787–1793.
[30] G. Wu, D.Y. Li, C.S. Dai, D.L. Wang, N. Li, Langmuir 24 (2008) 3566–3575.
[31] M.S. Saha, R.Y. Li, X.L. Sun, S.Y. Ye, Electrochem. Commun. 11 (2009) 438–441.
[32] L.P. Shi, Q.M. Gao, Y.H. Wu, Electroanalysis 21 (2009) 715–722.
[33] C.D. Liang, S. Dai, J. Am. Chem. Soc. 128 (2006) 5316–5317.
[34] Y.H. Wen, H.M. Zhang, P. Qian, H.P. Ma, B.L. Yi, Y.S. Yang, Chin. J. Chem. 25 (2007) 278–283.
[35] C.E. Banks, A. Crossley, C. Salter, S.J. Wilkins, R.G. Compton, Angew. Chem. Int. Ed. 45 (2006) 2533–2537.
[36] J.L. Figueiredo, M.F.R. Pereira, M.M.A. Freitas, J.J.M. Orfao, Carbon 37 (1999) 1379–1389.
[37] T.G. Ros, A.J. van Dillen, J.W. Geus, D.C. Koningsberger, Chem. Eur. J. 8 (2002) 1151–1162.
[38] D. Hulicova-Jurcakova, M. Kodama, S. Shiraishi, H. Hatori, Z.H. Zhu, G.Q. Lu, Adv. Funct. Mater. 19 (2009) 1800–1809.
[39] S. Kundu, T.C. Nagaiah, W. Xia, Y. Wang, S.V. Dommele, J.H. Bitter, M. Santa, G. Grundmeier, M. Bron, W. Schuhmann, M. Muhler, J. Phys. Chem. C 113 (2009) 14302–14310.
[40] P.H. Matter, L. Zhang, U.S. Ozkan, J. Catal. 239 (2006) 83–96.
[41] R. Arrigo, M. Havecker, R. Schlogl, D.S. Su, Chem. Commun. (2008) 4891–4893.
[42] E. Yeager, J. Mol. Catal. 38 (1986) 5–25.
[43] R.L. McCreery, Chem. Rev. 108 (2008) 2646–2687.
[44] B. Sljukic, C.E. Banks, R.G. Compton, J. Iran Chem. Soc. 2 (2005) 1–25.
[45] N.R. Vettorazzi, L. Sereno, M. Katoh, M. Ota, L. Otero, J. Electrochem. Soc. 155 (2008) F110–F115.
[46] G. Wu, R. Swaidan, D.Y. Li, N. Li, Electrochim. Acta 53 (2008) 7622–7629.
[47] B. Choi, H. Yoon, I.S. Park, J. Jang, Y.E. Sung, Carbon 45 (2007) 2496–2501.
[48] C. Leon, J.M. Solar, V. Calemma, L.R. Radovic, Carbon 30 (1992) 797–811.
[49] S. Maldonado, S. Morin, K.J. Stevenson, Carbon 44 (2006) 1429–1437.
[50] Q.H. Yang, W.H. Xu, A. Tomita, T. Kyotani, Chem. Mater. 17 (2005) 2940–2945.
[51] A. Gattrell, J. Qian, C. Stewart, P. Graham, B. MacDougall, Electrochim. Acta 51 (2005) 395–407.
[52] S.Y. Deng, G.Q. Jian, J.P. Lei, Z. Hu, H.X. Ju, Biosens. Bioelectron. 25 (2009) 373–377.